

**Intensification of North American megadroughts through surface
and dust aerosol forcing.**

BENJAMIN I COOK *

NASA Goddard Institute for Space Studies, NY, NY, USA

Lamont-Doherty Earth Observatory, Palisades, NY, USA

RICHARD SEAGER

Lamont-Doherty Earth Observatory, Palisades, NY, USA

RON L MILLER

NASA Goddard Institute for Space Studies, NY, NY, USA

JOSEPH A MASON

University of Wisconsin, Madison, WI, USA

* *Corresponding author address:* Benjamin I Cook, NASA Goddard Institute for Space Studies, 2880 Broadway, New York, NY 10025.
E-mail: bc9z@ldeo.columbia.edu

ABSTRACT

During the late Medieval Climate Anomaly (MCA, 1100-1500 C.E.), much of western North America experienced recurrent periods of drought spanning decades or longer. These ‘megadroughts’ had exceptional persistence compared to more recent events and many climate models have difficulty reproducing droughts of similar duration. We conduct a suite of general circulation model experiments to test the impact of reconstructed sea surface temperature (SST) and land surface forcing during the megadroughts. The land surface forcing is conceptualized as a set of dune mobilization boundary conditions, derived from available geomorphological evidence and modeled as increased bare soil area and a dust aerosol source over the Central Plains (105°E–95°E, 32°E–44°E). Cold tropical Pacific SST forcing and other MCA radiative forcings (solar, volcanoes, etc) stimulate warming and drying over the Central Plains, but can not reproduce the persistence of the megadroughts. In our simulation with additional forcing from dust aerosols, the dust increases the shortwave planetary albedo, reducing energy inputs to the surface and the planetary boundary layer. This energy deficit increases atmospheric stability, inhibiting vertical movement and convection which reduces cloud cover and subsequent precipitation over the Central Plains. To compare against available drought reconstructions for the MCA, we calculated the Palmer Severity Drought Index (PDSI) from our model runs. Droughts simulated in our scenario with dust aerosols have significantly longer persistence time scales than the model experiments with only SST and bare soil forcing. Specifically, inclusion of dust aerosols extends significant autocorrelation out to a lag of 3 years, matching the persistence of tree ring reconstructed estimates of PDSI during the MCA. Results from this study provide the first model based evidence that dust aerosol forcing and land surface changes can explain the persistence of the MCA megadroughts,

although uncertainties remain in the formulation of the boundary conditions and the future importance of these feedbacks as western North America moves into an anthropogenically warmer and drier world.

1. Introduction

During the late Medieval Climate Anomaly (MCA), hydroclimate in western North America and the Great Plains was defined largely by episodic droughts that typically persisted for multiple decades or longer (Cook et al. 2004, 2007, 2010; Herweijer et al. 2007; Stahle et al. 2007). These droughts had significant ecological and societal consequences, causing major disruptions in regional civilizations (e.g., Benson et al. 2007b,a; Douglass 1929) and leading to widespread vegetation mortality and dune mobilization (Forman et al. 2001; Hanson et al. 2010; Miao et al. 2007). These so called ‘megadroughts’ are not only unprecedented in the instrumental record, but are also largely absent in climate reconstructions of the last 500 years. With modern droughts already exacting significant societal costs (Cook et al. 2007), there is much interest in understanding the processes that drive the persistence of the MCA megadroughts and assessing the possibility of such droughts occurring in the future (Cook et al. 2010).

Investigations into the forcing of the megadroughts have focused primarily on the role of sea surface temperature (SST) forcing during the MCA, especially shifts in the tropical Pacific (Burgman et al. 2010; Seager et al. 2008a), the Atlantic (Oglesby et al. 2011), or both (Feng et al. 2008). Drought over the southern United States and Great Plains regions is favored by cold phases of the El Niño Southern Oscillation (ENSO) (i.e., La Niña conditions) and warm SSTs in the tropical Atlantic (e.g., Kushnir et al. 2010; Nigam et al. 2011; Schubert et al. 2009; Seager et al. 2005), and there is evidence in the paleorecord for cooler tropical Pacific SSTs during much of the MCA (Cobb et al. 2003). General circulation models (GCM), forced by either idealized (Feng et al. 2008) or reconstructed (Burgman et al.

2010; Seager et al. 2008a) SST fields can stimulate some drying over North America, but still have difficulty reproducing the magnitude and persistence of the MCA megadroughts.

Aside from remote SST-forced teleconnections, land surface feedbacks also play a critical role in modulating drought and hydroclimatic variability. For example, positive soil moisture feedbacks on precipitation have been identified in many regions of the world, including the Great Plains and central North America (e.g., Findell et al. 2011; Koster et al. 2004; Meng and Quiring 2010). More recently, work on the Dust Bowl drought of the 1930s points to land degradation (i.e., vegetation mortality, wind erosion, and dust aerosols) acting as an amplifier of regional drought (Cook et al. 2008, 2009). In those studies, *Cook et. al.* found that inclusion of dust aerosols and reduced vegetation cover caused significant warming and drying over the Great Plains, increasing the fidelity of their simulated Dust Bowl temperature and precipitation anomalies. Precipitation reductions occurred via the well-established ‘Charney’ mechanism (Charney 1975; Charney et al. 1977), relating increased albedo (in our case from dust aerosols) to increased shortwave reflectance and reductions in net radiative fluxes at the surface and top of the atmosphere. With less energy available to drive vertical movement of the atmosphere, convection and precipitation were subsequently reduced. Conceptually, the Charney feedback is similar to the mechanism elucidated by Neelin and Held (1987), where an energy deficit at the surface must be balanced by decreases in energy export through increased subsidence and reductions in vertical movement and convection. These feedbacks may be especially important to consider for the MCA megadroughts, given the large-scale vegetation mortality, wind erosion, and dust aerosol transport that occurred during this interval, as inferred from records of paleo-dunes (Forman et al. 2001; Hanson et al. 2010; Miao et al. 2007).

To date, however, the impact of the dune mobilization, vegetation mortality, and dust aerosols on the MCA megadroughts is understudied. While several papers have speculated that these landscape impacts may have amplified these droughts (Feng et al. 2008; Seager et al. 2008b), only one study to date has explicitly tested surface impacts on the megadroughts within a modeling framework (Cook et al. 2011). They found that vegetation mortality alone (i.e., without wind erosion or dust feedbacks) was insufficient to amplify the model-simulated droughts or reproduce the drought persistence seen in the paleorecord. Here, we expand on the experiments of Cook et al. (2011), presenting a new ensemble of simulations including wind erosion and dust aerosol forcing. We frame our analysis around two questions: 1) Can forcing from dune mobilization, conceptualized as reduced vegetation coverage and a dust aerosol source, intensify simulated MCA megadroughts? and 2) Does inclusion of these surface factors increase the simulated persistence of these megadroughts?

2. Methods and Data

a. North American Drought Atlas

We use information on drought history in North America from the North America Drought Atlas (NADA) version 2a (Cook et al. 2004, 2007), a gridded ($2.5^\circ \times 2.5^\circ$) tree ring based reconstruction of the Palmer Drought Severity Index (PDSI, Palmer 1965) for boreal summer (June-July-August, JJA). PDSI is a locally normalized index of drought that incorporates both moisture supply (precipitation) and demand (evaporation as a function of temperature) in its calculation. Positive values of PDSI indicate wetter than normal conditions and

negative values indicate drier than normal conditions. Despite the JJA focus of the NADA, PDSI has a memory timescale of about 12 months, allowing it to incorporate information on temperature and precipitation throughout the year. PDSI from the NADA has been used with good success in a variety of modeling studies investigating historical and paleodroughts over North America (e.g., Cook et al. 2011; Herweijer et al. 2006, 2007; Oglesby et al. 2011; Seager et al. 2008a)

b. Model Description

For our experiments, we used a version of the Goddard Institute for Space Studies (GISS) atmospheric GCM ‘ModelE’ (Schmidt et al. 2006), extensively updated in preparation for experiments as part of the Fifth Assessment Report of the Intergovernmental Panel on Climate Change). This current version has a horizontal resolution of $2^\circ \times 2.5^\circ$ latitude/longitude with 40 vertical layers in the atmosphere. Each land cell is divided into vegetated and bare soil columns with six vertical layers that extend to a maximum depth of 3.5 meters (heat and moisture budgets are calculated separately for each soil column). Vegetation is prescribed using Matthews (1983), and photosynthesis and stomatal conductance parameterizations are based on Farquhar et al. (1980) and Ball et al. (1987), respectively. Included within ModelE is a mineral dust aerosol model (Miller et al. 2006). In the default setup, dust aerosols are emitted to the atmosphere as a function of soil moisture and wind speed from the source map of Ginoux et al. (2001), representing sediment filled topographic depressions that persist over geologic time scales. Once airborne, dust aerosols alter the radiative budget within the atmosphere, increasing shortwave reflection and longwave absorption. In the current version

of the model, dust aerosols have no microphysical interactions. Studies using the the immediately preceding version of the model have demonstrated the ability of ModelE to produce high fidelity simulations of the modern day climate, including historical trends and variability (Hansen et al. 2007; Schmidt et al. 2006). Over North America, SST teleconnections are well resolved, and a variety of studies have successfully used ModelE to investigate twentieth century hydroclimate variability over this region (e.g., Cook et al. 2008, 2009; Ruiz-Barradas and Nigam 2006).

c. Boundary Conditions

For our historical ensemble (1857-2005 C.E., described below) we use SST forcing from the Kaplan et al. (1998) dataset. For our MCA ensembles (1321-1461 C.E.), the SST forcing is prescribed using a coral based SST reconstruction for the tropical Pacific (30°S-30°N) (Cobb et al. 2003). Oxygen isotope anomalies for the MCA portion of the Cobb et al. (2003) coral record are calculated relative to the monthly climatology for 1886-1998 C.E. SST anomalies are calculated for low (≥ 6 years) and high (<6) frequency components of the record separately, based on regressions against the Kaplan et al. (1998) dataset. Outside the tropical Pacific, SSTs are taken from the model runs of Seager et al. (2008a). In their experiments, Seager et al. (2008a) prescribed the Cobb et al. (2003) reconstruction in the tropical Pacific, coupling these SSTs elsewhere to a thermodynamic mixed layer ocean. SSTs outside the tropical Pacific therefore reflect the influence of tropical Pacific variability communicated primarily through atmospheric teleconnections. Annual SST anomalies in the NINO 3.4 region, calculated relative to the 1857-2005 C.E. mean from Kaplan et al.

(1998), indicate a cooler than normal ENSO state during the late MCA (Figure 1a). Further information on the SST reconstruction and calculation can be found in Seager et al. (2008a), Burgman et al. (2010), and the Supplemental Material of Cook et al. (2011).

The geologic record provides evidence for widespread and recurrent dune mobilization events during the MCA (Forman et al. 2001; Hanson et al. 2010; Miao et al. 2007), with the most recent events likely occurring during the fourteenth and fifteenth centuries. These events were driven primarily by megadrought induced vegetation mortality and reductions in vegetation cover. In the Nebraska Sand Hills, stratigraphic evidence shows that aeolian sand mobilization coincided with water table drawdown during the MCA (Mason et al. 2004). More generally, moisture availability for vegetation is likely to be the predominant control on dune mobility in the Great Plains. The sand-transporting potential of modern winds is high by global standards, but dunes are largely stable at present because precipitation is sufficient to maintain vegetation cover (Muhs and Maat 1993). Large uncertainties remain, however, regarding the specific timing, duration, and extent of the vegetation mortality and associated wind erosion and dust aerosol forcing, making it difficult to develop quantitative boundary forcings for our model experiments. For our MCA runs, we prescribed our dune mobilization region (Figure 1b) over the Central Plains (105°E–95°E, 32°E–44°E), based qualitatively on maps and evidence from geomorphological analyses (Forman et al. 2001; Hanson et al. 2010; Miao et al. 2007). For the model, we translated this to 1) a 50% reduction in vegetation cover (simulating the vegetation mortality) and 2) a new dust aerosol emission source added to the default source map of Ginoux et al. (2001).

To validate wind erosion and dust aerosol emissions from this new source, we estimated aeolian deposition in two areas: 98°W–100°W, 40°–42°N (Area 1) and 96°W–98°W, 40°–42°N

(Area 2). Application of optically stimulated luminescence dating to thick source-proximal loess sections with high resolution has demonstrated that major intervals of rapid Holocene loess accumulation were synchronous across the central Plains (Miao et al. 2007). A discrete increment of loess deposited between 1100 and 1400 C.E. is consistently present, forming about 5-13% of the total Holocene loess thickness. Thinner Holocene loess forms a relatively uniform mantle over uplands in the areas chosen for validation (30-60 cm thick in Area 1 and 24-36 cm thick in Area 2, based on observations by Jacobs and Mason (2007) and soil surveys), allowing estimation of deposition rates at spatial scales comparable to model resolution. We assume that the loess in those areas was preserved with minimal resuspension after deposition. Taking into account the ranges of total thickness and assuming 5-13% of that total was deposited between 1100 and 1400 C.E., we derive average aeolian deposition rates over the period 1100-1400 C.E. of $80\text{-}380\text{ g m}^{-2}\text{ yr}^{-1}$ and $60\text{-}230\text{ g m}^{-2}\text{ yr}^{-1}$ for Areas 1 and 2, respectively. We use these deposition rates to validate the dust emissions from the new Central Plains source in our model scenario. Because of time uncertainties in our boundary conditions, including the SST reconstruction, we cannot directly compare our simulated droughts against specific drought events in the record. Instead, we compare our simulated droughts (1321-1461 C.E.) against general drought statistics from the NADA for the MCA (1100-1500 C.E.) and the post-MCA (1501-2000 C.E.) periods.

d. Model Experiments

Our experiments are comprised of four, 5-member ensemble simulations using ModelE (Table 1). Each experiment is based on a set of unique forcing, land surface, and SST boundary

conditions, and each ensemble member is initialized using different initial states for the atmosphere and land surface. Our base run is SST-MOD, a historical (1857-2005 C.E.) control run forced with observational period climate forcings (i.e., solar, volcanic, greenhouse gases) and SSTs prescribed according to Kaplan et al. (1998). Unless otherwise indicated, all anomalies for the MCA model ensembles are calculated relative to the ensemble mean for 1857-2005 C.E. from SST-MOD. All MCA model ensembles are forced with transient, reconstructed estimates of forcing from greenhouse gas concentrations, solar variability, volcanic aerosols, and the reconstructed tropical Pacific SSTs from 1321-1461 C.E. In SST-Only, we use the default land surface and MCA SST forcing only. In SST+BSOIL, we use the MCA SST forcing and our 50% bare soil boundary condition over the Central Plains, but with no Central Plains dust aerosol source, following Cook et al. (2011). Our final full effect ensemble, SST+BSOIL+DUST, includes the SST forcing, Central Plains bare soil, and the new Central Plains dust source. We focus the bulk of our model and paleoclimate analyses on the Central Plains region where we prescribed the MCA land surface boundary conditions (i.e., the bare soil fraction and dust source). All significance testing is based on a two-sided Student's t-test with a significance threshold of $p \leq 0.05$.

3. Results

a. Model Validation

For the Central Plains region, we compared the monthly climatology (1961-1990 C.E.) of temperature and precipitation from the ensemble mean of our SST-MOD experiment against

observations (1961-1990 C.E.) from the Climate Research Unit (CRU) climate grids version 2.1 (Mitchell and Jones 2005) (Figure 2). ModelE reproduces the amplitude and seasonality of climate over this region, including the seasonal peak in precipitation during the late spring and early summer (May-August). Major biases only occur in two months: April (positive) and September (negative).

Ensembles annual average dust deposition from the SST+BSOIL+DUST ensemble is 152 (+/-35 st. dev.) $\text{g m}^{-2} \text{ yr}^{-1}$ and 82 (+/-19 st. dev.) $\text{g m}^{-2} \text{ yr}^{-1}$ for Areas 1 and 2, respectively. This places our dust source emissions at the low end of our observed range, but within the same order of magnitude, suggesting that the simulated climate impact of dust in our SST+BSOIL+DUST ensemble is conservative. Given the uncertainties inherent in estimating these boundary conditions, we consider this a reasonable first-order estimate of the dust forcing during the MCA.

b. PDSI in the North American Drought Atlas

During the MCA (Figure 3a), the Central Plains experienced multiple decadal or longer periods of drought that were largely absent in the post-MCA time period (Figure 3b). This persistence is clearly seen in the autocorrelation of the PDSI calculated in the NADA, which shows significant autocorrelation of the MCA PDSI out to lags of 9 years (Figure 4a). In contrast, persistence in the post-MCA PDSI is similar and significant only at a lag of 1 year (Figure 4b). To remove the impact of changes in the mean PDSI on the persistence calculation, we re-calculated the autocorrelation functions for the MCA (Figure 4c) and post-MCA PDSI (Figure 4d) after adjusting the means of both time series to zero. Even

with this adjustment, MCA PDSI retains significant persistence at time lags of 1, 2, 3, and 8 years, supporting the contention that, relative to recent periods, droughts during the MCA were largely unprecedented in their duration and persistence.

c. Model Precipitation and Temperature Response

All three MCA model scenarios show significant warming and drying over the Central Plains relative to the SST-MOD ensemble (Figure 5). In SST-Only (blue bars), these anomalies are largest during summer and fall (June–November). The winter and cold season responses in SST-Only are muted and largely insignificant, despite the cold tropical Pacific SST forcing and the expectation that ENSO impacts would be largest during these months. Our Central Plains region, however, expands beyond the northern edge of the region of strongest La Niña–precipitation teleconnections, and may not respond as strongly as southwest and northwest North America, which show the expected dry and wet winter response, respectively (not shown). Notably, our winter and summer precipitation anomalies are similar in magnitude and spatial extent when compared to a recent millennium run of the Community Climate System Model forced with solar, volcanic, and greenhouse gas forcing estimates and a coupled ocean (Landrum et al. in review). This suggests that the background drying during summer may be less a consequence of SST variability and more due to external top of the atmosphere forcing during the MCA.

Warming in SST+BSOIL (green bars) is significantly increased beyond the SST forcing in May–October; dust aerosols in SST+BSOIL+DUST (brown bars) further enhance the warming in March–April and June–July–August (JJA). SST+BSOIL leads to a minor en-

hancement of the drying during July, but the impact of the increased bare soil beyond the SST forcing is insignificant otherwise. Dust aerosol forcing in June, however, leads to significant drying beyond SST-Only and SST+BSOIL, nearly doubling the precipitation anomaly of SST-Only. The SST+BSOIL and SST+BSOIL+DUST scenarios have their strongest impact during the summer season, when their enhancement of the warming and drying beyond SST-Only is largest. With this in mind, we focus the remainder of our analyses on the temperature response during JJA and the precipitation response during June.

Spatially, SST-Only leads to significant surface warming and drying over the Central Plains and much of eastern North America (Figure 6a,b). This warming is enhanced over the Central Plains in SST+BSOIL (Figure 6c), but the June precipitation response (Figure 6d) is similar to SST-Only. Dust aerosol forcing in SST+BSOIL+DUST further enhances the warming over the Central Plains (Figure 6e), and leads to moderate increases in temperature over a wider region. The dust aerosols intensify the drying over the Central Plains (Figure 6f), and also lead to some moderate drying in the southern Plains and Texas. The wider spatial scale of the climate response to the dust aerosols is likely due to the response to the dust aerosol forcing spreading out spatially over at least a Rossby radius of deformation. All three scenarios show substantial temporal variability (Figure 7). Temperatures in SST+BSOIL and SST+BSOIL+DUST are, in general, consistently warmer than SST-Only (Figure 7a). Mean surface temperatures in SST+BSOIL and SST+BSOIL+DUST are significantly warmer than SST-Only by +0.53 and +0.79 K, respectively (Figure 8a). Maximum temperature increases are largest in the SST+BSOIL scenarios (Figure 8c), but dust aerosol forcing leads to significant increases in minimum temperatures beyond either SST-Only or SST+BSOIL (Figure 8d) due to dust inhibition of infrared cooling by the surface at night

(see next section). Precipitation in SST+BSOIL+DUST is generally lower than in the other MCA simulations (Figure 7b), but periods of near normal precipitation are interspersed with exceptionally dry intervals. The very dry intervals generally coincide with especially cold SST forcing (Figure 1a) (e.g., 1350-1370 C.E., 1380-1410 C.E.), implying that the dust aerosols amplify externally forced drought conditions. Precipitation in SST+BSOIL+DUST during June is significantly suppressed, on average, by an additional $-0.16 \text{ mm day}^{-1}$ over SST-Only; the SST+BSOIL difference is insignificant (Figure 8b).

d. Surface Fluxes (JJA)

Increases in maximum temperatures are driven primarily through shifts in the surface energy balance: declines in latent heating (Figure 9a) related to increases in the surface sensible heat flux (Figure 9b). Reduced vegetation cover in SST+BSOIL and SST+BSOIL+DUST reduces transpiration, the flux of moisture through the leaves of plants. This leads to an overall decline in evapotranspiration and latent heat flux, largely balanced by increases in sensible heating. Sensible heat flux anomalies in the SST+BSOIL+DUST experiment are muted compared to SST+BSOIL: the addition of the dust aerosols reduces surface heating through increased shortwave reflection, reducing incident solar inputs at the surface (Figure 9c). Maximum temperature still increases, however, because the reduced latent heat flux reduction is still large relative to the sensible heat flux. Because dust aerosols are effective absorbers of infrared radiation (Figure 9d), they trap outgoing longwave radiation at night, insulating the surface and increasing minimum temperatures.

e. Surface Responses (June)

Primarily through increases in albedo and shortwave reflection, both SST+BSOIL and SST+BSOIL+DUST lead to decreases in net radiation incident upon the surface (Figure 10a). For SST+BSOIL, the albedo increase comes from the increased bare soil coverage which tends to have a higher shortwave albedo than vegetation. In SST+BSOIL+DUST, the albedo increase is from a combination of increased surface albedo from the bare soil and increased shortwave reflection from the dust aerosols. The energy deficit at the surface reduces planetary boundary layer heights (Figure 10b) and decreases the daytime peak boundary layer lapse rate (Figure 10c). The boundary layer responses lead to increased stability, inhibiting vertical motion of air parcels and significantly reducing convective cloud cover (Figure 10d) and precipitation. The radiative perturbation is only large enough to reduce precipitation beyond SST-Only forcing in the SST+BSOIL+DUST experiment.

f. PDSI in the MCA Simulations

We calculated PDSI using surface temperature and precipitation from our model simulations in order to evaluate our modeled drought persistence and compare against the PDSI from the NADA. We calculated the PDSI for every grid cell over the Central Plains region separately, standardizing against the normal period defined by our SST-MOD ensemble (1857-2005), and then averaging over the Central Plains. Soil moisture capacity for the top and bottom layers was set to 25.4 mm (1 in.) and 127 mm (5 in.). Evapotranspiration was calculated as a function of temperature based on Thornthwaite (1948), the same method used to derive the PDSI that forms the foundation of the NADA reconstruction.

Ensemble mean Central Plains PDSI time series for JJA are shown in Figure 11, the same season represented by the NADA. All three models produce recurrent periods of summer drought, but only the SST+BSOIL+DUST ensemble is able to simulate droughts with durations comparable to results from the NADA PDSI analysis (Figure 3a). This increased persistence is indicated by the autocorrelation function (Figure 12). Based on the unadjusted PDSI time series, the SST+BSOIL+DUST scenario is the only run that simulates significant persistence out to a period of 10 years (Figure 12c), although it may be overestimated relative to the NADA. If the PDSI time series are adjusted to a zero mean, however, the SST+BSOIL+DUST autocorrelation function aligns quite closely with the NADA function, and is the only one of our three MCA scenarios with significant persistence at time lags of 1, 2, and 3 years.

4. Discussion and Conclusions

Drought is a recurrent and societally relevant climate phenomena in much of North America, especially in the western half of the continent. From 1980–2003, droughts caused \$144 billion in damages and lost production (Cook et al. 2007; Ross and Lott 2003), accounting for 41% of the total cost of all weather related disasters during this period (Ross and Lott 2003). Even while acknowledging the significant costs and disruptions associated with modern droughts, it is sobering to realize that their durations are relatively short compared to the events that occurred during the MCA. With available evidence supporting a trajectory towards a drier mean state in the future (e.g., Seager et al. 2007), it is worth investigating the causes of the MCA megadroughts, and whether these factors will play a role in a potentially drier future.

Our experiments show that estimated tropical Pacific SSTs and increased bare soil associated with dune mobilization are not sufficient to reproduce the drying and persistence of the MCA megadroughts over the Central Plains. The SST forcing leads to some modest precipitation reductions relative to our modern ensemble; the addition of the bare soil leads to significant warming, but does not amplify this drying. Only when dust aerosols are included does the model respond with drying that leads to significant precipitation reductions and droughts that are much more persistent, matching the autocorrelation structure of the droughts recorded in the NADA. At this point, it is unclear what the mechanism is for increased persistence from the dust aerosols seen in the zero-mean adjusted model PDSI. In the real world, persistence would arise from vegetation mortality due to dust induced drying, further increasing wind erosion and feeding back to sustain dune mobilization, wind erosion, and dry conditions. Our model, however, lacks the capability to fully simulate these dynamical interactions. The distribution of the mean adjusted PDSI for the SST+BSOIL+DUST simulation shows flatter and broader peak than for SST-Only, indicating a tendency to distribute further away from the mean. In quantitative terms, this translates to an excess kurtosis of -0.29 and -0.44 for SST-Only and SST+BSOIL+DUST, respectively. While not quite bimodal, it does fit with expected dust-precipitation interactions. When precipitation is lower, drier soils favor increased wind erosion which further reduce precipitation. When precipitation is higher, increased soil moisture inhibits wind erosion, reducing the impact of the dust aerosols on precipitation and favoring overall wetter conditions.

Our results are promising, and support the idea that land surface feedbacks from aeolian activity during the MCA played an important role reinforcing the megadroughts. These feedbacks have been hinted at previously in studies of the Dust Bowl (Cook et al. 2008, 2009),

the only observational era drought with land degradation and aeolian activity approaching the same scale as the megadroughts. Even more so than for the Dust Bowl, however, large uncertainties remain in both the timing and magnitude of drought forcings during the MCA. Further refinement of the land surface boundary condition estimates, especially the time uncertainties, would allow for better comparisons between the model simulations and specific events. For SSTs, additional proxies from corals or sediment records in the Pacific and Atlantic would help decrease uncertainties and increase the spatial coverage of the SST reconstructions in these basins. We also note that, due to limitations of ModelE, we were forced to prescribe the land surface changes and dust aerosol source as time invariant boundary conditions. In the real world, the vegetation, aeolian system, and climate system are tightly coupled, and we would expect the droughts to initiate independently (e.g., from SST forcing), driving the vegetation mortality and wind erosion that would feedback to amplify the original drought. Even without using a coupled framework, however, our experiments provide strong evidence that these factors, especially the dust aerosols, can explain the persistence of the megadroughts.

In the short term, the land surface dynamics that amplified the megadroughts and Dust Bowl are unlikely to play a major role in the intensification of future droughts. During the Dust Bowl, much of the dust storm activity originated from small farms with few erosion control measures and annual crops that were extremely vulnerable to moisture deficits. The initiation of this drought, forced by cold SSTs in the tropical Pacific (Schubert et al. 2004; Seager et al. 2008b), caused widespread crop failures over the Central and Southern Plains, exposing highly erodible top soil. In response, the United States government formed the Soil Conservation Service with the goal of preventing the same level of land degradation

from occurring again (Hansen and Libecap 2004). The program was successful and, as a result, subsequent droughts (e.g., 1948-1957, 1998-2004) avoided the same levels of wind erosion and dust storm activity, despite severe moisture deficits. Besides erosion measures, irrigation in the west has also expanded rapidly since the 1950s (Wisser et al. 2010), providing additional sources of water that have enabled farmers to be more resistant to drought events. Other than farmlands, much of the region is composed of pastures and grasslands that host perennial grasses evolutionarily adapted to the hydroclimatic variability in the region and capable of surviving at least short term droughts. There is evidence, though, that grasslands in some regions will respond to longer term droughts (Evans et al. 2011), and that livestock grazing activities may make these systems more vulnerable (Van Auken 2000). As the twenty-first centuries progresses, various factors will affect the resilience of agricultural and natural systems in the region, and the potential for landscape feedbacks to drought. On one side, both greenhouse gas forced drying trends (Seager et al. 2007) and the continued depletion of non-renewable groundwater resources (e.g., Sophocleous 2010) will increase drought stress on natural ecosystems and agricultural systems. Conversely, the direct effect of increased atmospheric carbon dioxide concentrations on plant physiology may serve to actually increase plant resistance to water stress and drought (e.g., Morgan et al. 2011). The future of hydroclimate and landscape processes in the Central Plains and western North America will thus likely depend on the complex interplay of climate dynamics, ecosystem responses, and direct human management.

Acknowledgments.

The authors acknowledge the support of NSF grant ATMO9-02716, NOAA grant NA100AR-4310137, NSF Grant ATM-06-20066, as well as the National Aeronautics and Space Administration Atmospheric Composition Program.

REFERENCES

- Ball, J., I. Woodrow, and J. Berry, 1987: A model predicting stomatal conductance and its application to the control of photosynthesis under different environmental conditions. *Progress in Photosynthesis*, I. Biggins, Ed., Martinus Nijhoff Publishers, 221–224.
- Benson, L., M. Berry, E. Jolie, J. Spangler, D. Stahle, and E. Hattori, 2007a: Possible impacts of early-11th-, middle-12th-, and late-13th-century droughts on western Native Americans and the Mississippian Cahokians. *Quaternary Science Reviews*, **26 (3-4)**, 336–350.
- Benson, L., K. Petersen, and J. Stein, 2007b: Anasazi (Pre-Columbian Native-American) Migrations During The Middle-12Th and Late-13th Centuries–Were they Drought Induced? *Climatic Change*, **83 (1)**, 187–213.
- Burgman, R., R. Seager, A. Clement, and C. Herweijer, 2010: Role of tropical Pacific SSTs in global medieval hydroclimate: A modeling study. *Geophysical Research Letters*, **37 (6)**, L06 705.
- Charney, J., 1975: Dynamics of deserts and drought in the Sahel. *Quarterly Journal of the Royal Meteorological Society*, **101 (428)**, 193–202.
- Charney, J., W. Quirk, S. Chow, and J. Kornfield, 1977: A Comparative Study of the Effects of Albedo Change on Drought in Semi-Arid Regions. *Journal of Atmospheric Sciences*, **34**, 1366–1385.

- Cobb, K., C. Charles, H. Cheng, and R. Edwards, 2003: El Nino/Southern Oscillation and tropical Pacific climate during the last millennium. *Nature*, **424 (6946)**, 271–276.
- Cook, B., R. Miller, and R. Seager, 2008: Dust and sea surface temperature forcing of the 1930s “Dust Bowl” drought. *Geophysical Research Letters*, **35 (8)**, L08710.
- Cook, B., R. Miller, and R. Seager, 2009: Amplification of the North American “Dust Bowl” drought through human-induced land degradation. *Proceedings of the National Academy of Sciences*, **106 (13)**, 4997.
- Cook, B., R. Seager, and R. Miller, 2011: The impact of devegetated dune fields on north american climate during the late medieval climate anomaly. *Geophysical Research Letters*, **38 (14)**, L14704.
- Cook, E., R. Seager, M. Cane, and D. Stahle, 2007: North American drought: Reconstructions, causes, and consequences. *Earth Science Reviews*, **81 (1-2)**, 93–134.
- Cook, E., R. Seager, R. Heim Jr, R. Vose, C. Herweijer, and C. Woodhouse, 2010: Megadroughts in North America: placing IPCC projections of hydroclimatic change in a long-term palaeoclimate context. *Journal of Quaternary Science*, **25 (1)**, 48–61.
- Cook, E., C. Woodhouse, C. Eakin, D. Meko, and D. Stahle, 2004: Long-Term Aridity Changes in the Western United States. *Science*, **306 (5698)**, 1015–1018.
- Douglass, A., 1929: The secret of the southwest solved by talkative tree rings: Natl. *National Geographic*, **56 (6)**, 736–770.
- Evans, S. E., K. M. Byrne, W. K. Lauenroth, and I. C. Burke, 2011: Defining the limit to

- resistance in a drought-tolerant grassland: long-term severe drought significantly reduces the dominant species and increases ruderals. *Journal of Ecology*, **99** (6), 1500–1507, doi:10.1111/j.1365-2745.2011.01864.x, URL <http://dx.doi.org/10.1111/j.1365-2745.2011.01864.x>.
- Farquhar, G., S. Caemmerer, and J. Berry, 1980: A biochemical model of photosynthetic CO₂ assimilation in leaves of C₃ species. *Planta*, **149** (1), 78–90.
- Feng, S., R. Oglesby, C. Rowe, D. Loope, and Q. Hu, 2008: Atlantic and Pacific SST influences on Medieval drought in North America simulated by the Community Atmospheric Model. *Journal of Geophysical Research*, **113** (D11).
- Findell, K., P. Gentine, B. Lintner, and C. Kerr, 2011: Probability of afternoon precipitation in eastern united states and mexico enhanced by high evaporation. *Nature Geoscience*, **4** (7), 434–439.
- Forman, S., R. Oglesby, and R. Webb, 2001: Temporal and spatial patterns of Holocene dune activity on the Great Plains of North America: megadroughts and climate links. *Global and Planetary Change*, **29** (1-2), 1–29.
- Ginoux, P., M. Chin, I. Tegen, J. Prospero, B. Holben, O. Dubovik, and S. Lin, 2001: Sources and distributions of dust aerosols simulated with the gocart model. *Journal of Geophysical Research*, **106** (D17), 20 255–20.
- Hansen, J., et al., 2007: Climate simulations for 1880–2003 with GISS ModelE. *Climate Dynamics*, **29** (7), 661–696.

- Hansen, Z. and G. Libecap, 2004: Small Farms, Externalities, and the Dust Bowl of the 1930s. *Journal of Political Economy*, **112 (3)**, 665–694.
- Hanson, P., A. Arbogast, W. Johnson, R. Joeckel, and A. Young, 2010: Megadroughts and late Holocene dune activation at the eastern margin of the Great Plains, north-central Kansas, USA. *Aeolian Research*, **1 (3-4)**, 101–110.
- Herweijer, C., R. Seager, and E. Cook, 2006: North American droughts of the mid to late nineteenth century: a history, simulation and implication for Mediaeval drought. *The Holocene*, **16 (2)**, 159.
- Herweijer, C., R. Seager, E. Cook, and J. Emile-Geay, 2007: North American Droughts of the Last Millennium from a Gridded Network of Tree-Ring Data. *Journal of Climate*, **20 (7)**, 1353–1376.
- Jacobs, P. and J. Mason, 2007: Late quaternary climate change, loess sedimentation, and soil profile development in the central great plains: A pedosedimentary model. *Geological Society of America Bulletin*, **119 (3-4)**, 462–475.
- Kaplan, A., M. Cane, Y. Kushnir, A. Clement, M. Blumenthal, and B. Rajagopalan, 1998: Analyses of global sea surface temperature 1856-1991. *Journal of Geophysical Research*, **103 (18)**, 567–18.
- Koster, R., et al., 2004: Regions of strong coupling between soil moisture and precipitation. *Science*, **305 (5687)**, 1138–1141.
- Kushnir, Y., R. Seager, M. Ting, N. Naik, and J. Nakamura, 2010: Mechanisms of Tropical

- Atlantic SST Influence on North American Hydroclimate Variability. *Journal of Climate*, **23**, 5610–5628.
- Landrum, L., B. Otto-Bliesner, E. Wahl, A. Conley, P. Lawrence, and H. Teng, in review: Last millennium climate and its variability in ccsm4. *Journal of Climate*.
- Mason, J., J. Swinehart, R. Goble, and D. Loope, 2004: Late-holocene dune activity linked to hydrological drought, nebraska sand hills, usa. *The Holocene*, **14 (2)**, 209–217.
- Matthews, E., 1983: Global Vegetation and Land Use: New High-Resolution Data Bases for Climate Studies. *Journal of Climate and Applied Meteorology*, **22 (3)**, 474–487.
- Meng, L. and S. Quiring, 2010: Observational relationship of sea surface temperatures and precedent soil moisture with summer precipitation in the us great plains. *International Journal of Climatology*, **30 (6)**, 884–893.
- Miao, X., J. Mason, J. Swinehart, D. Loope, P. Hanson, R. Goble, and X. Liu, 2007: A 10,000 year record of dune activity, dust storms, and severe drought in the central Great Plains. *Geology*, **35 (2)**, 119.
- Miller, R., et al., 2006: Mineral dust aerosols in the NASA Goddard Institute for Space Sciences ModelE atmospheric general circulation model. *J. Geophys. Res*, **111**, D06 208.
- Mitchell, T. and P. Jones, 2005: An improved method of constructing a database of monthly climate observations and associated high-resolution grids. *Int. J. Climatol*, **25 (6)**, 693–712.

- Morgan, J., et al., 2011: C4 grasses prosper as carbon dioxide eliminates desiccation in warmed semi-arid grassland. *Nature*, **476 (7359)**, 202–205.
- Muhs, D. and P. Maat, 1993: The potential response of eolian sands to greenhouse warming and precipitation reduction on the great plains of the usa. *Journal of Arid Environments*, **25 (4)**, 351–361.
- Neelin, J. and I. Held, 1987: Modeling tropical convergence based on the moist static energy budget. *Monthly Weather Review*, **115**, 3.
- Nigam, S., B. Guan, and A. Ruiz-Barradas, 2011: Key role of the atlantic multidecadal oscillation in 20th century drought and wet periods over the great plains. *Geophysical Research Letters*, **38 (16)**, L16 713.
- Oglesby, R., S. Feng, Q. Hu, and C. Rowe, 2011: The role of the atlantic multidecadal oscillation on medieval drought in north america: Synthesizing results from proxy data and climate models. *Global and Planetary Change*, "" (0), –, doi:10.1016/j.gloplacha.2011.07.005, URL <http://www.sciencedirect.com/science/article/pii/S0921818111001172>.
- Palmer, W., 1965: Meteorological drought, Research Paper No. 45. *US Weather Bureau, Washington, DC*, **58**.
- Ross, T. and N. Lott, 2003: A climatology of 1980-2003 extreme weather and climate events. Tech. rep., NOAA/NESDIS. National Climatic Data Center, Asheville, NC.
- Ruiz-Barradas, A. and S. Nigam, 2006: IPCC's Twentieth-Century Climate Simulations:

- Varied Representations of North American Hydroclimate Variability. *Journal of Climate*, **19 (16)**, 4041–4058.
- Schmidt, G., et al., 2006: Present-day atmospheric simulations using GISS ModelE: Comparison to in situ, satellite, and reanalysis data. *Journal of Climate*, **19 (2)**, 153–192.
- Schubert, S., M. Suarez, P. Pegion, R. Koster, and J. Bacmeister, 2004: On the Cause of the 1930s Dust Bowl. *Science*, **303 (5665)**, 1855–1859.
- Schubert, S., et al., 2009: A US CLIVAR Project to Assess and Compare the Responses of Global Climate Models to Drought-Related SST Forcing Patterns: Overview and Results. *Journal of Climate*, **22 (19)**, 5251–5272.
- Seager, R., R. Burgman, Y. Kushnir, A. Clement, E. Cook, N. Naik, and J. Miller, 2008a: Tropical Pacific forcing of North American medieval megadroughts: Testing the concept with an atmosphere model forced by coral-reconstructed SSTs. *Journal of Climate*, **21 (23)**, 6175–6190.
- Seager, R., Y. Kushnir, C. Herweijer, N. Naik, and J. Velez, 2005: Modeling of Tropical Forcing of Persistent Droughts and Pluvials over Western North America: 1856–2000. *Journal of Climate*, **18 (19)**, 4065–4088.
- Seager, R., Y. Kushnir, M. Ting, M. Cane, N. Naik, and J. Miller, 2008b: Would Advance Knowledge of 1930s SSTs Have Allowed Prediction of the Dust Bowl Drought? *Journal of Climate*, **21 (13)**, 3261–3281.
- Seager, R., et al., 2007: Model projections of an imminent transition to a more arid climate

in southwestern North America. *Science*, **316** (DOI: [10.1126/science.1139601](https://doi.org/10.1126/science.1139601)), 1181–1184.

Sophocleous, M., 2010: Review: groundwater management practices, challenges, and innovations in the High Plains aquifer, USA—lessons and recommended actions. *Hydrogeology Journal*, **18** (3), 559–575.

Stahle, D., F. Fye, E. Cook, and R. Griffin, 2007: Tree-ring reconstructed megadroughts over north america since ad 1300. *Climatic change*, **83** (1), 133–149.

Thorntwaite, C., 1948: An approach toward a rational classification of climate. *Geographical review*, **38** (1), 55–94.

Van Auken, O., 2000: Shrub invasions of north american semiarid grasslands. *Annual Review of Ecology and Systematics*, **31**, 197–215.

Wisser, D., B. Fekete, C. Vorosmarty, and A. Schumann, 2010: Reconstructing 20th century global hydrography: a contribution to the Global Terrestrial Network-Hydrology (GTN-H). *Hydrol. Earth Syst. Sci*, **14**, 1–24.

List of Tables

- 1 Summary of model experiments conducted as part of this study.

All experiments represent 5-member ensembles, with each ensemble initialized using a unique set of starting conditions. For each simulation, the table indicates the years over which the ensembles were run, the source of the SST forcing, and if bare soil (BSOIL) or dust source (DUST) boundary conditions were included.

30

TABLE 1. Summary of model experiments conducted as part of this study. All experiments represent 5-member ensembles, with each ensemble initialized using a unique set of starting conditions. For each simulation, the table indicates the years over which the ensembles were run, the source of the SST forcing, and if bare soil (BSOIL) or dust source (DUST) boundary conditions were included.

Experiment	Years	SSTs	Dune, Bare Soil	Dune, Dust
SST-MOD	1857-2005	Kaplan et al. (1998)	–	–
SST-Only	1321-1461	Cobb et al. (2003)	–	–
SST+BSOIL	1321-1461	Cobb et al. (2003)	+	–
SST+BSOIL+DUST	1321-1461	Cobb et al. (2003)	+	+

List of Figures

- 1 NINO 3.4 sea surface temperature (SST) anomalies (a) and dune mobilization region (b) for the MCA experiments. All MCA experiments (SST-Only, SST+BSOIL, SST+BSOIL+DUST) use the same SST forcing, based on a coral reconstruction of SSTs in the tropical Pacific. Anomalies are relative to the 1856-2005 mean SSTs in the NINO3.4 region from the Kaplan SST dataset. Dune mobilization region is used to define the 50% bare soil area in the SST+BSOIL and SST+BSOIL+DUST experiments and the dust source region in the SST+BSOIL+DUST experiment. 35
- 2 Monthly temperature (a) and precipitation (b) climatology (1961-1990) for the Central Plains region (105°W-95°W, 32°N-44°N), calculated from our modern day SST forced ensemble and the CRU 2.1 climate grids (green line). 36
- 3 Summer season (June-July-August, JJA) PDSI anomalies from the North American Drought Atlas (NADA), averaged over the Central Plains region (105°W-95°W, 32°N-44°N). Droughts in this region during the late Medieval Climate Anomaly (MCA) (a) were generally more persistent than droughts after 1500 C.E. (b). Both time series were smoothed with a 5-year low pass (lowess spline) filter. 37

- 4 Autocorrelation function (ACF) for Central Plains PDSI from the NADA. Droughts during the MCA (a) have significant persistence (grey line, $p \leq 0.05$) out to a lag of -9 years. Post-MCA drought persistence (b) is significantly reduced, with significant persistence only at a lag of -1 year. Even after standardizing to zero mean, the MCA PDSI (c) retains significant persistence at lags of -1, -2, -3, and -8 years, while the post-MCA PDSI (d) is relatively unchanged. 38
- 5 Ensemble mean monthly temperature (K) (a) and precipitation (mm day^{-1}) (b) response over the Central Plains region (105°W - 95°W , 32°N - 44°N), in our SST-Only (blue bars), SST+BSOIL (green bars), and SST+BSOIL+DUST (brown bars) experiments, relative to SST-MOD. Anomalies significant different from SST-MOD (Student's two-side t-test, $p \leq 0.05$) are indicated with a *. 39
- 6 Ensemble mean monthly surface temperature (JJA, K) (a,c,e) and precipitation (June, mm day^{-1}) (b,d,f) responses over North American in our MCA model runs. The central Plains region (105°W - 95°W , 32°N - 44°N) is outlined in the black dashes. Cells with insignificant ($p \geq 0.05$) differences between the MCA runs and SST-MOD have been masked out. 40
- 7 Ensemble mean time series of mean monthly surface temperature (JJA, K) (a) and precipitation (June, mm day^{-1}) (b) responses over North American in our MCA model runs, averaged over the Central Plains region (105°W - 95°W , 32°N - 44°N). All time series have been smoother with a 5-year low pass (lowess) filter. 41

- 8 Normalized histograms of (a) mean monthly surface temperature (JJA, K), (b) precipitation (June, mm day⁻¹), (c) mean monthly maximum surface temperature (JJA, K), and (d) mean monthly minimum surface temperature (JJA, K) responses over North American in our MCA model runs, averaged over the Central Plains region (105°W-95°W, 32°N-44°N). 42
- 9 Normalized histograms of JJA surface flux (W m⁻²) responses averaged over the Central Plains region (105°W-95°W, 32°N-44°N): (a) latent heat flux, (b) sensible heat flux, (c) incident shortwave flux at the surface, and (d) downwelling longwave flux at the surface. 43
- 10 Normalized histograms of mean June surface climate responses averaged over the Central Plains region (105°W-95°W, 32°N-44°N): (a) net radiation at the surface (W m⁻²), (b) planetary boundary layer height (meters), (c) peak lapse rate in the planetary boundary layer (K km⁻¹), and (d) convective cloud cover (% normal departure). 44
- 11 Ensemble average summer season (JJA) PDSI calculated from our MCA and averaged over the Central Plains region (105°W-95°W, 32°N-44°N): (a) SST-Only, (b) SST+BSOIL, and (c) SST+BSOIL+DUST. PDSI anomalies for all MCA runs were normalized relative to 1857-2005 C.E. from the SST-MOD ensemble. 45

12 Autocorrelation function (ACF) for the ensemble average JJA Central Plains PDSI (105°W-95°W, 32°N-44°N) from the SST-Only (a), SST+BSOIL (b), and SST+BSOIL+DUST (c) model runs. PDSI in the SST+BSOIL+DUST ensemble, driven by the dust aerosol forced drying, is the only scenario that can generate significant persistence at time scales similar to the MCA PDSI from the NADA. Even after the adjustment to zero mean (d,e,f), SST+BSOIL+DUST is the only the scenario with significant persistence at lags of -2 and -3 years, similar to the autocorrelation of the adjusted NADA PDSI. 46

Model Boundary Conditions

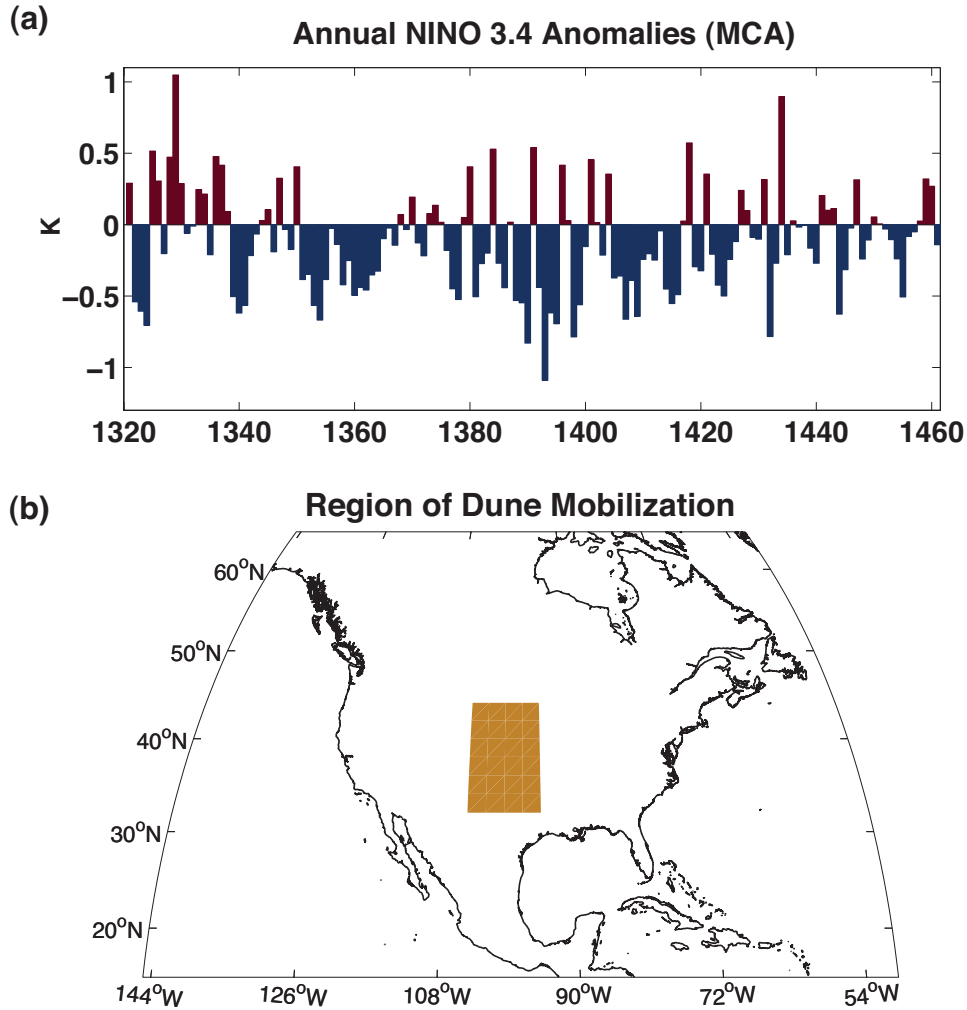


FIG. 1. NINO 3.4 sea surface temperature (SST) anomalies (a) and dune mobilization region (b) for the MCA experiments. All MCA experiments (SST-Only, SST+BSOIL, SST+BSOIL+DUST) use the same SST forcing, based on a coral reconstruction of SSTs in the tropical Pacific. Anomalies are relative to the 1856-2005 mean SSTs in the NINO3.4 region from the Kaplan SST dataset. Dune mobilization region is used to define the 50% bare soil area in the SST+BSOIL and SST+BSOIL+DUST experiments and the dust source region in the SST+BSOIL+DUST experiment.

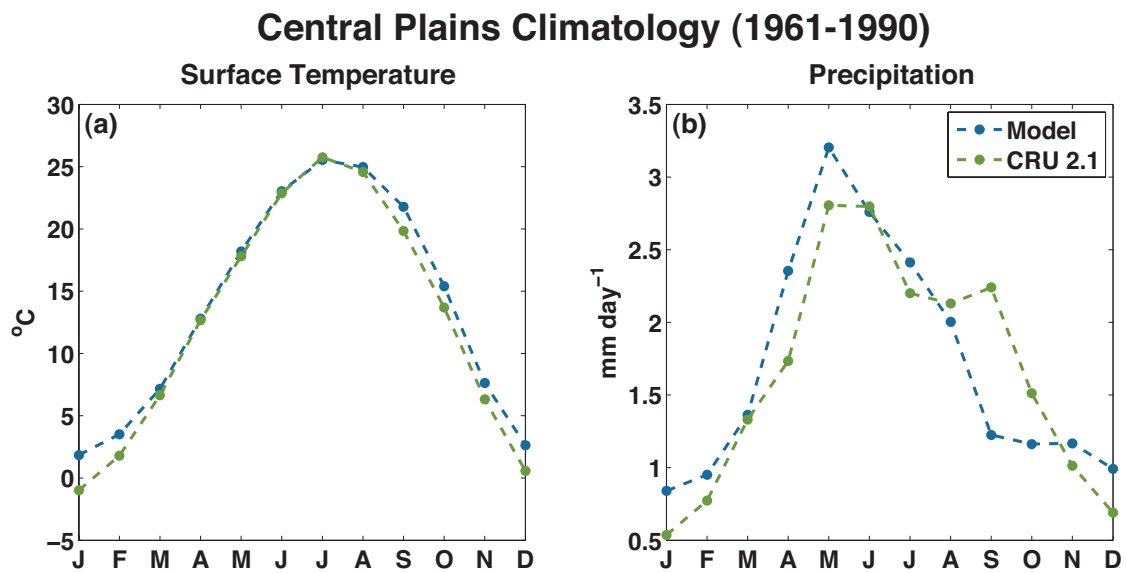


FIG. 2. Monthly temperature (a) and precipitation (b) climatology (1961-1990) for the Central Plains region (105°W-95°W, 32°N-44°N), calculated from our modern day SST forced ensemble and the CRU 2.1 climate grids (green line).

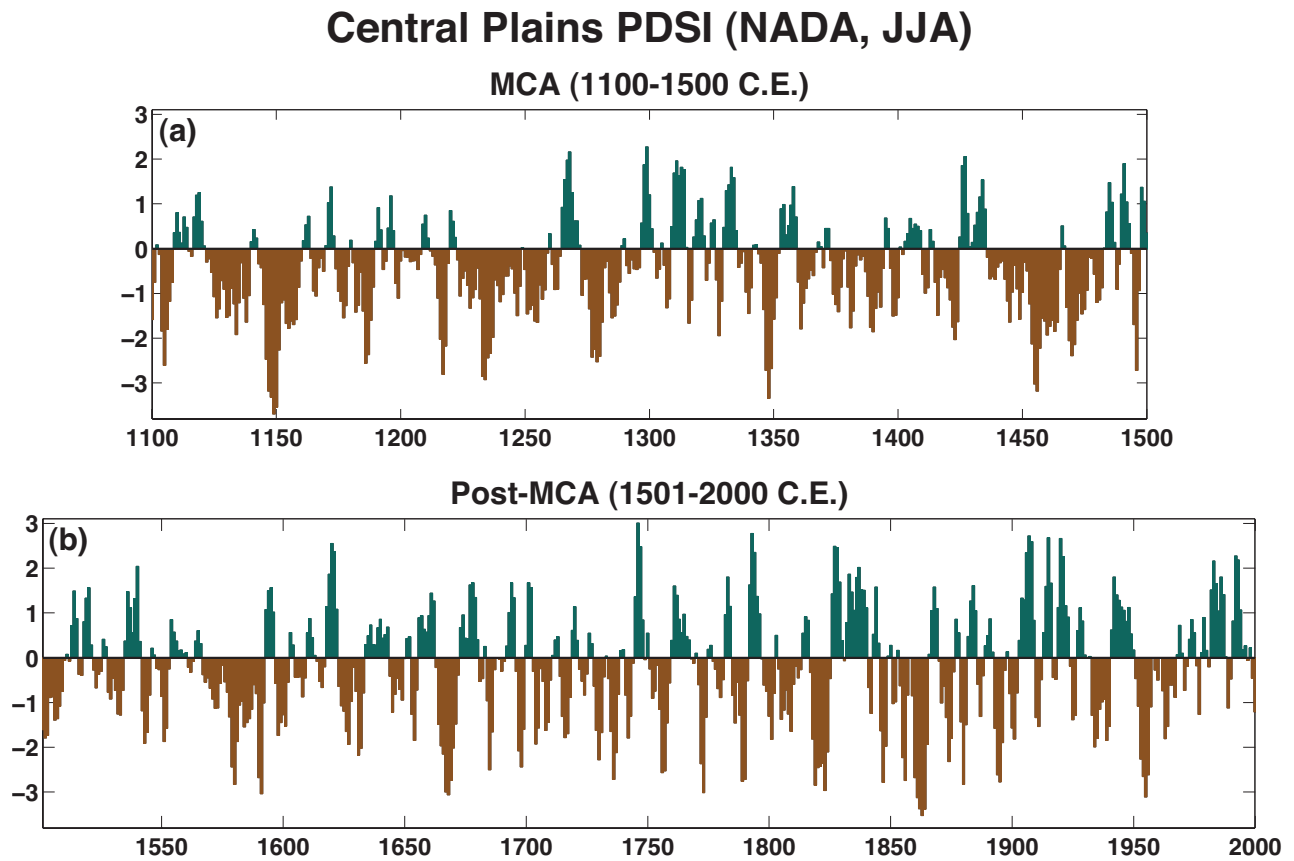


FIG. 3. Summer season (June-July-August, JJA) PDSI anomalies from the North American Drought Atlas (NADA), averaged over the Central Plains region (105°W - 95°W , 32°N - 44°N). Droughts in this region during the late Medieval Climate Anomaly (MCA) (a) were generally more persistent than droughts after 1500 C.E. (b). Both time series were smoothed with a 5-year low pass (lowess spline) filter.

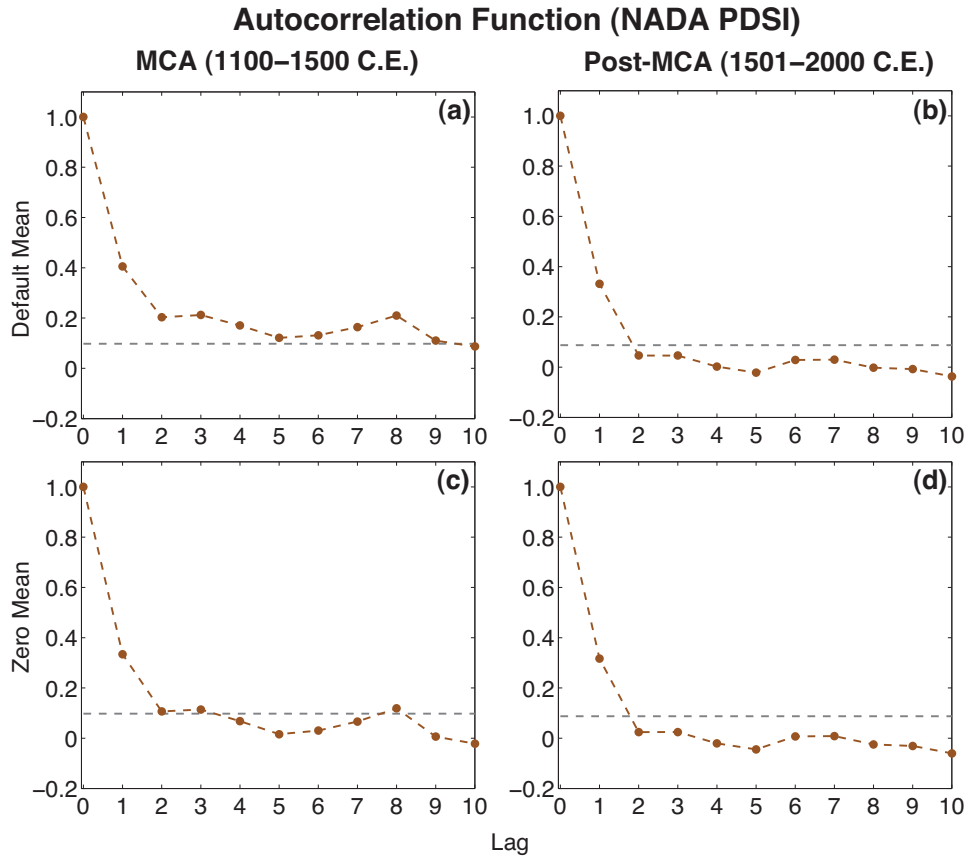


FIG. 4. Autocorrelation function (ACF) for Central Plains PDSI from the NADA. Droughts during the MCA (a) have significant persistence (grey line, $p \leq 0.05$) out to a lag of -9 years. Post-MCA drought persistence (b) is significantly reduced, with significant persistence only at a lag of -1 year. Even after standardizing to zero mean, the MCA PDSI (c) retains significant persistence at lags of -1, -2, -3, and -8 years, while the post-MCA PDSI (d) is relatively unchanged.

Central Plains ΔT and ΔP , vs SST-MOD Surface Temperature

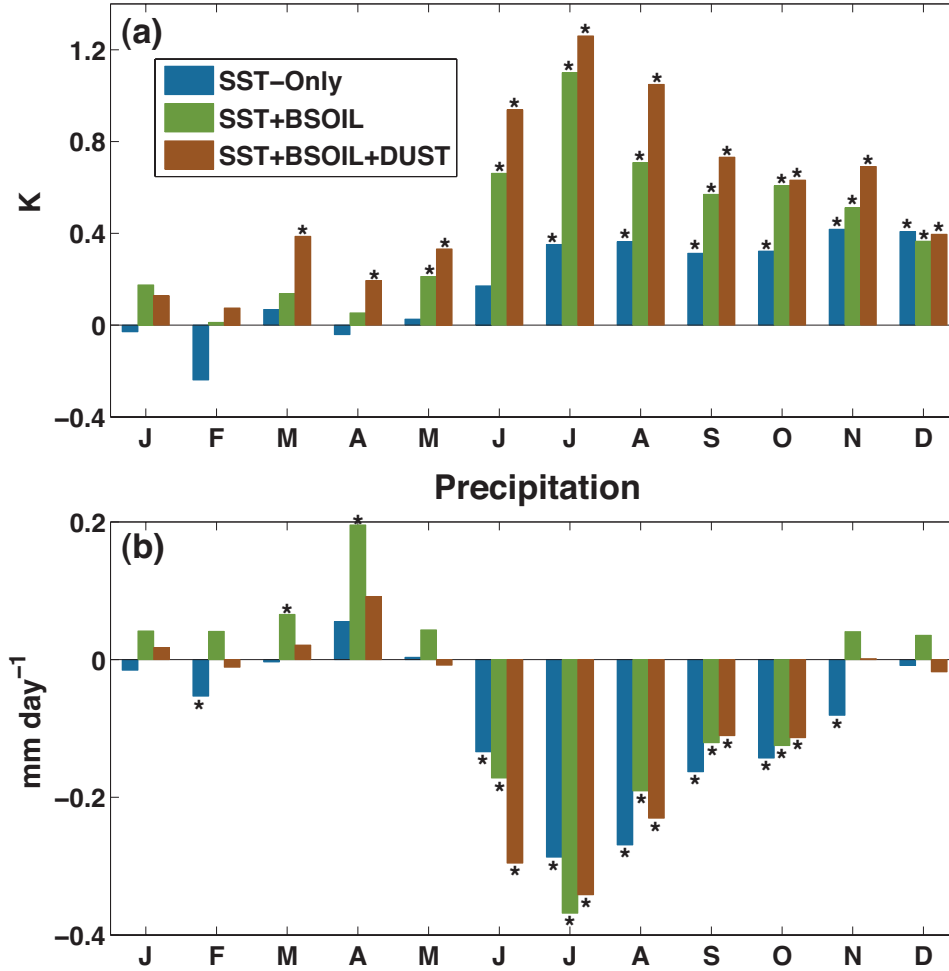


FIG. 5. Ensemble mean monthly temperature (K) (a) and precipitation (mm day⁻¹) (b) response over the Central Plains region (105°W-95°W, 32°N-44°N), in our SST-Only (blue bars), SST+BSOIL (green bars), and SST+BSOIL+DUST (brown bars) experiments, relative to SST-MOD. Anomalies significant different from SST-MOD (Student's two-side t-test, $p \leq 0.05$) are indicated with a *.

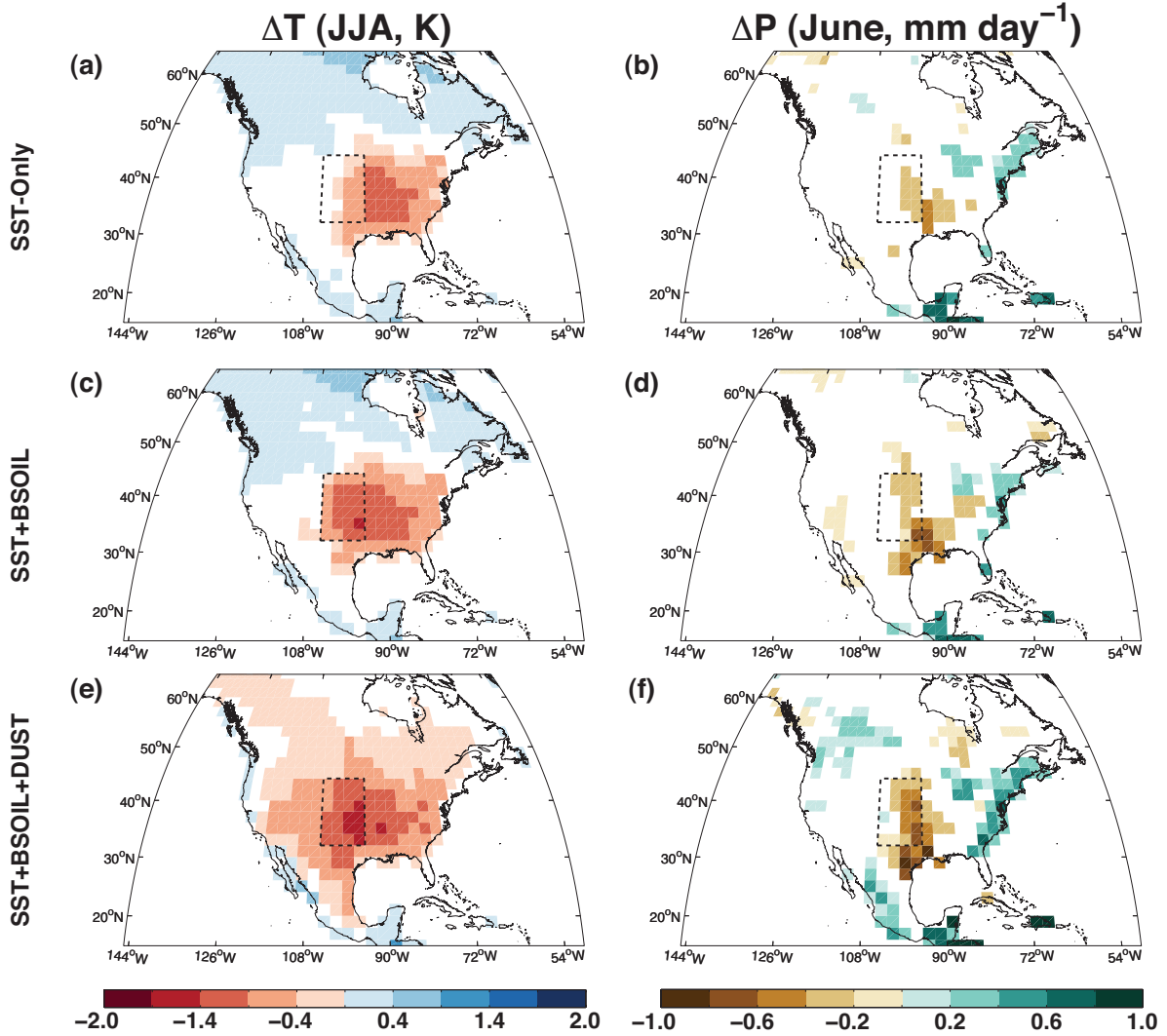


FIG. 6. Ensemble mean monthly surface temperature (JJA, K) (a,c,e) and precipitation (June, mm day^{-1}) (b,d,f) responses over North American in our MCA model runs. The central Plains region (105°W - 95°W , 32°N - 44°N) is outlined in the black dashes. Cells with insignificant ($p \geq 0.05$) differences between the MCA runs and SST-MOD have been masked out.

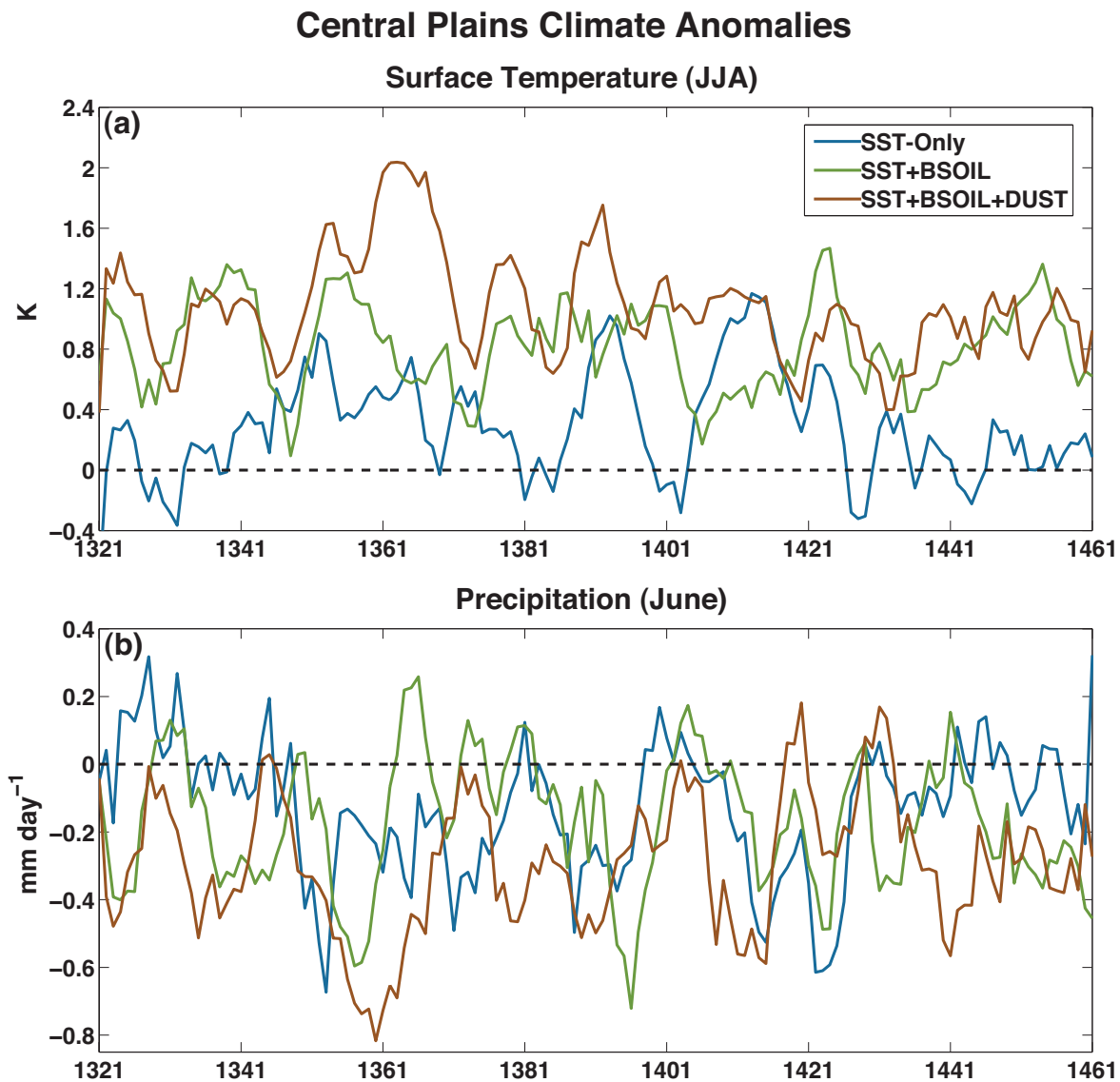


FIG. 7. Ensemble mean time series of mean monthly surface temperature (JJA, K) (a) and precipitation (June, mm day^{-1}) (b) responses over North American in our MCA model runs, averaged over the Central Plains region (105°W - 95°W , 32°N - 44°N). All time series have been smoother with a 5-year low pass (lowess) filter.

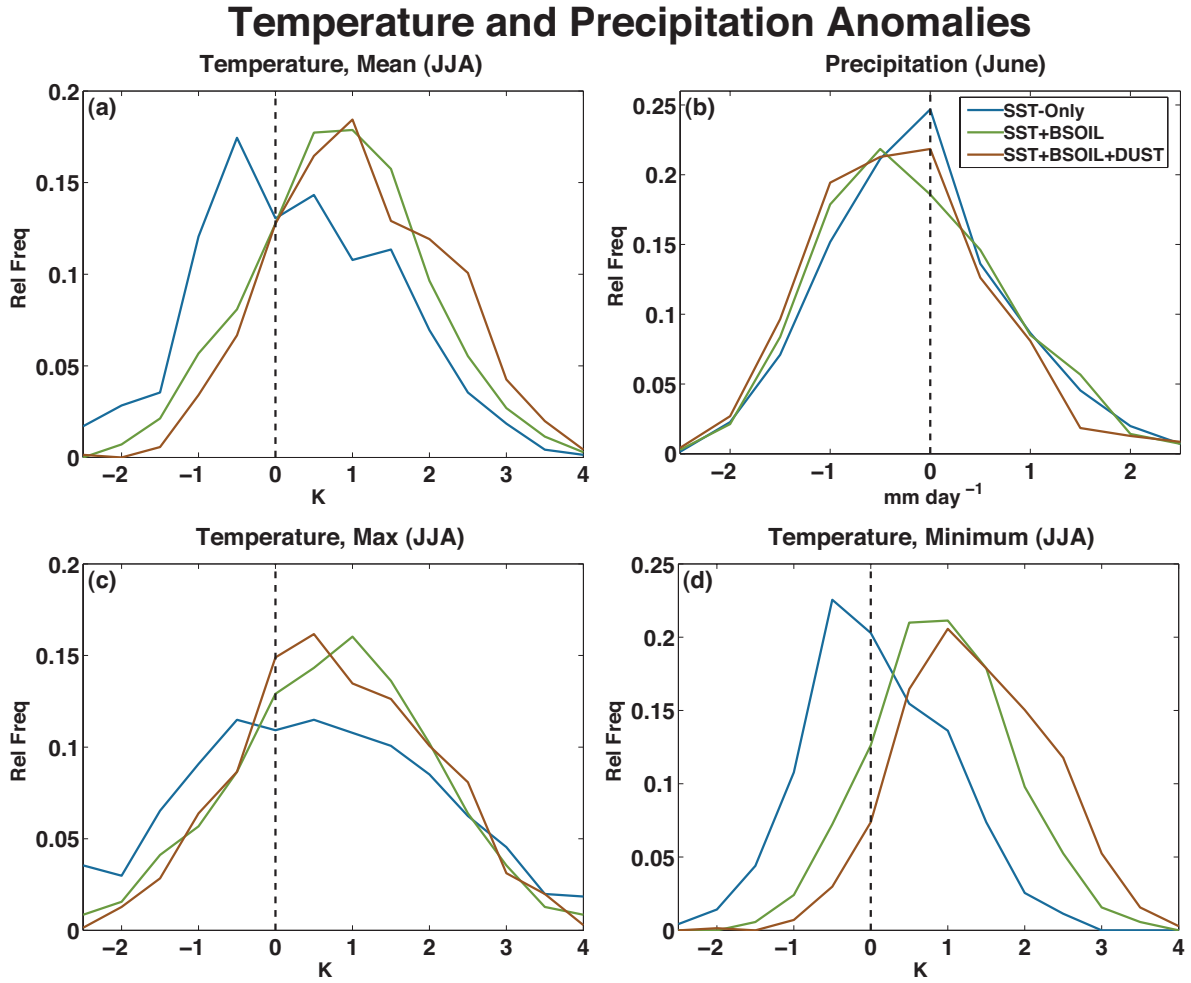


FIG. 8. Normalized histograms of (a) mean monthly surface temperature (JJA, K), (b) precipitation (June, mm day⁻¹), (c) mean monthly maximum surface temperature (JJA, K), and (d) mean monthly minimum surface temperature (JJA, K) responses over North American in our MCA model runs, averaged over the Central Plains region (105°W-95°W, 32°N-44°N).

Surface Fluxes (JJA)

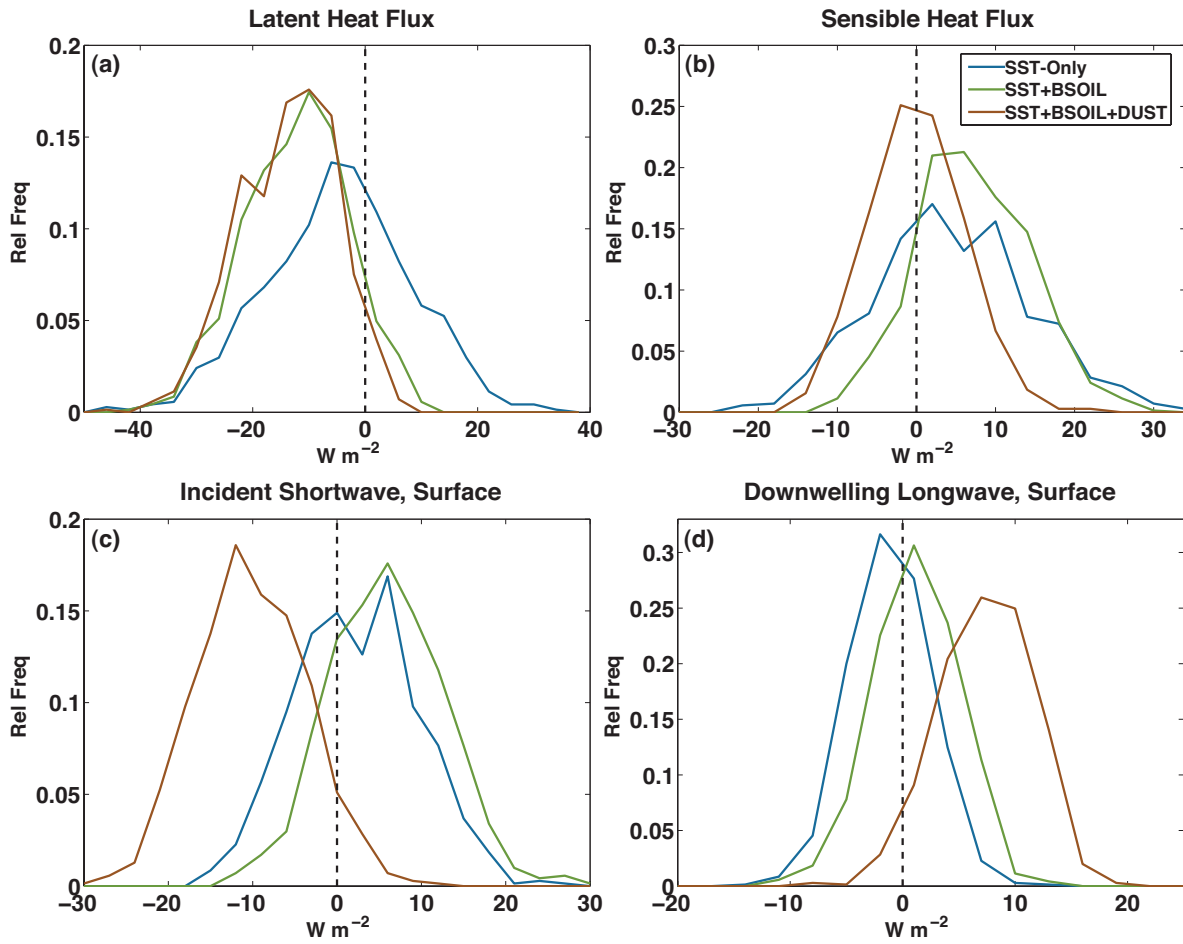


FIG. 9. Normalized histograms of JJA surface flux (W m^{-2}) responses averaged over the Central Plains region (105°W - 95°W , 32°N - 44°N): (a) latent heat flux, (b) sensible heat flux, (c) incident shortwave flux at the surface, and (d) downwelling longwave flux at the surface.

Surface Response (June)

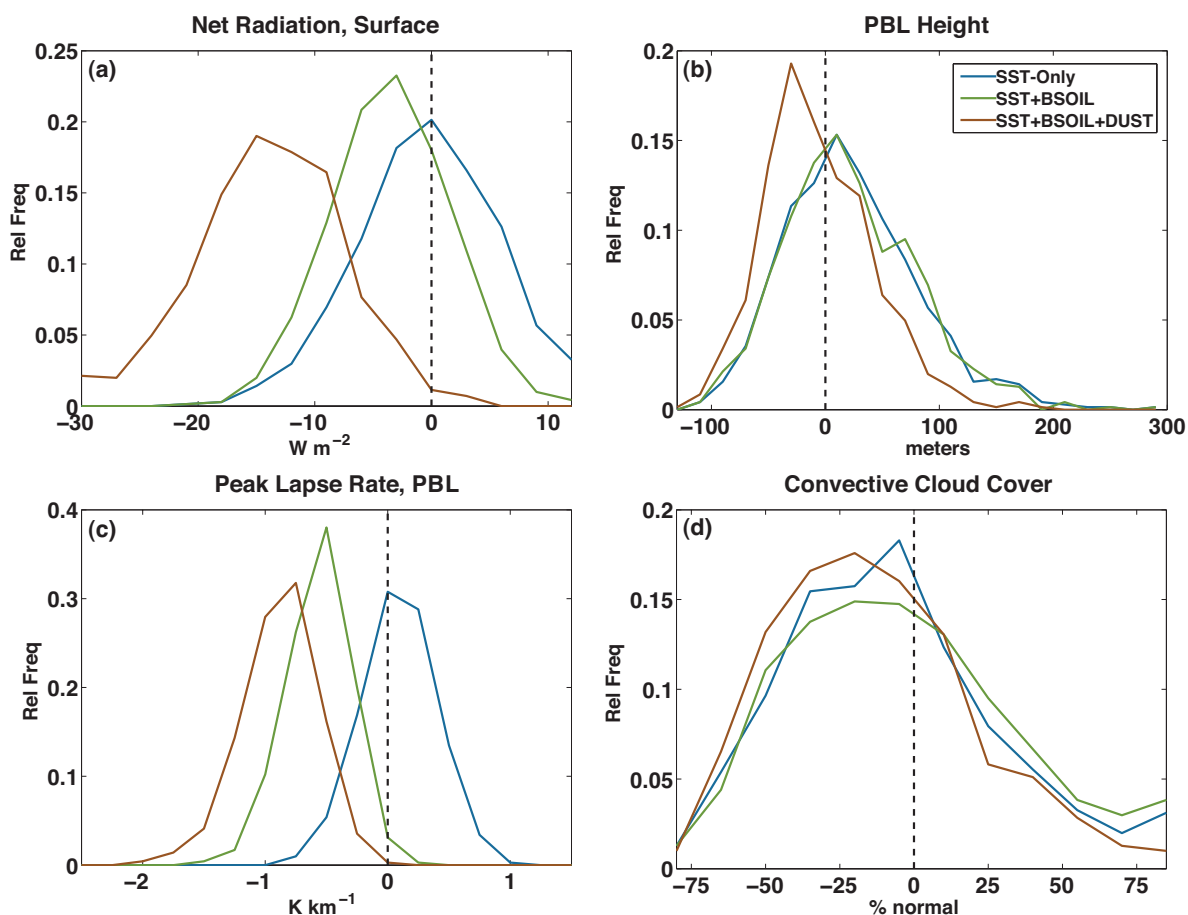


FIG. 10. Normalized histograms of mean June surface climate responses averaged over the Central Plains region ($105^{\circ}W$ - $95^{\circ}W$, $32^{\circ}N$ - $44^{\circ}N$): (a) net radiation at the surface ($W m^{-2}$), (b) planetary boundary layer height (meters), (c) peak lapse rate in the planetary boundary layer ($K km^{-1}$), and (d) convective cloud cover (% normal departure).

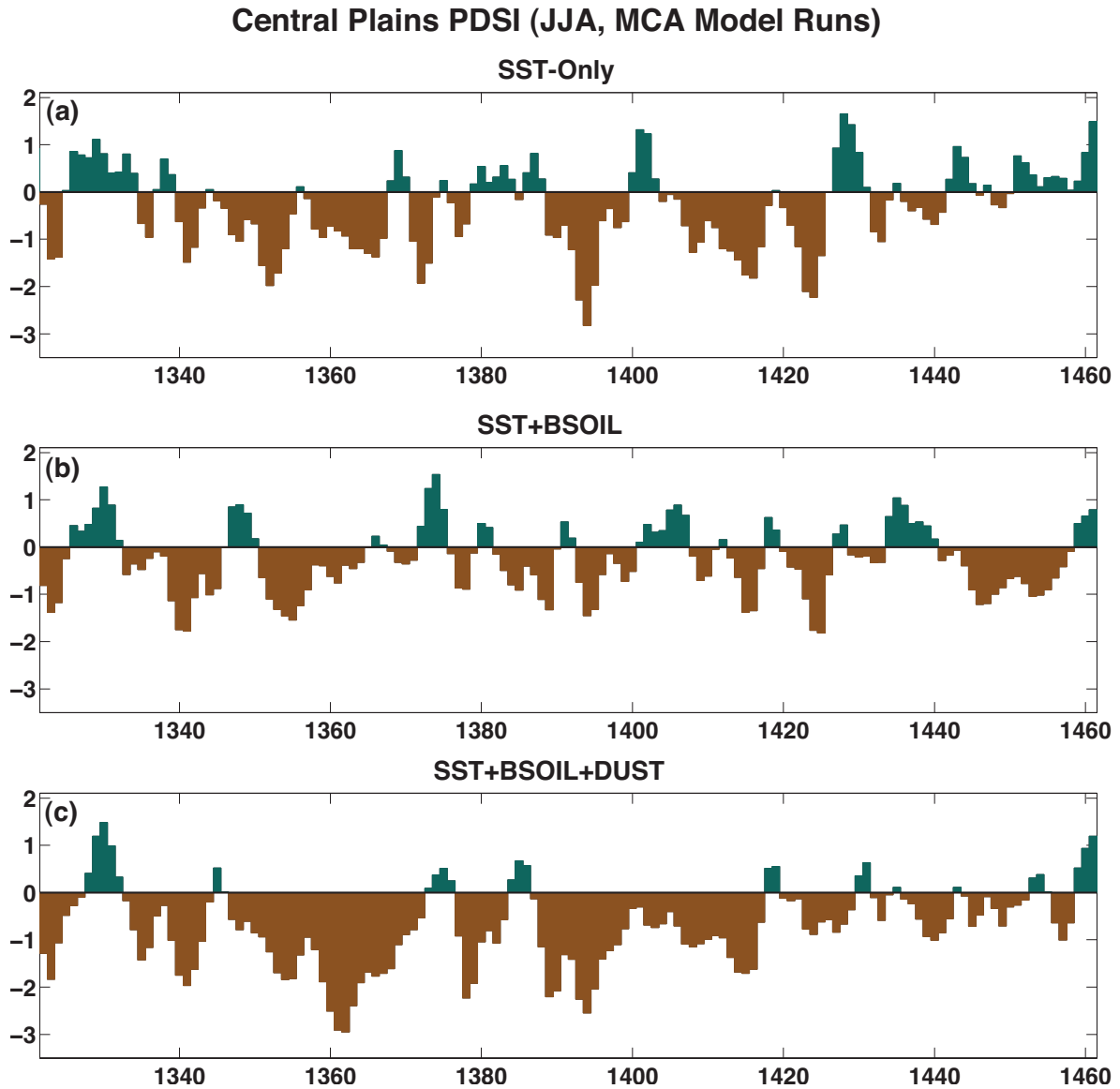


FIG. 11. Ensemble average summer season (JJA) PDSI calculated from our MCA and averaged over the Central Plains region (105°W - 95°W , 32°N - 44°N): (a) SST-Only, (b) SST+BSOIL, and (c) SST+BSOIL+DUST. PDSI anomalies for all MCA runs were normalized relative to 1857-2005 C.E. from the SST-MOD ensemble.

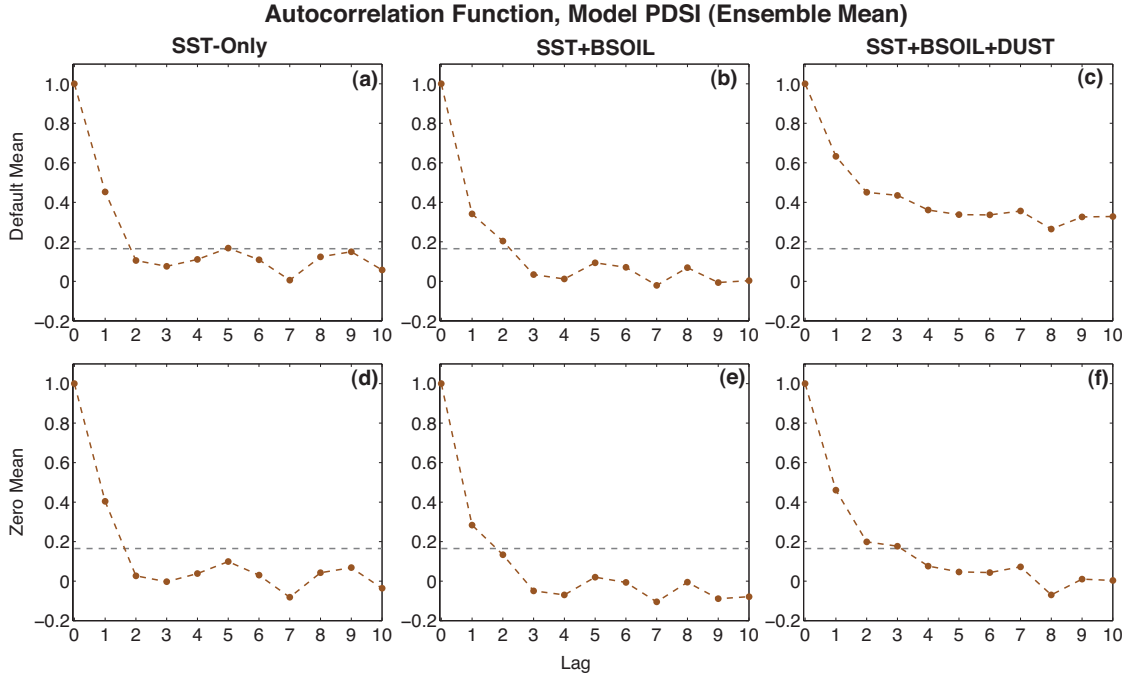


FIG. 12. Autocorrelation function (ACF) for the ensemble average JJA Central Plains PDSI (105°W - 95°W , 32°N - 44°N) from the SST-Only (a), SST+BSOIL (b), and SST+BSOIL+DUST (c) model runs. PDSI in the SST+BSOIL+DUST ensemble, driven by the dust aerosol forced drying, is the only scenario that can generate significant persistence at time scales similar to the MCA PDSI from the NADA. Even after the adjustment to zero mean (d,e,f), SST+BSOIL+DUST is the only the scenario with significant persistence at lags of -2 and -3 years, similar to the autocorrelation of the adjusted NADA PDSI.